

LETTER

Liquid demixing in elastic networks: Cavitation, permeation, or size selection?

To cite this article: Pierre Ronceray *et al* 2022 *EPL* **137** 67001

View the [article online](#) for updates and enhancements.

You may also like

- [Liquid–liquid phase separation driven compartmentalization of reactive nucleoplasm](#)

Rabia Laghmach and Davit A Potoyan

- [Light scattering microscopy measurements of single nuclei compared with GPU-accelerated FDTD simulations](#)

Julian Stark, Thomas Rothe, Steffen Kieß et al.

- [Coupling of living cells with external electrical stimulation: a computational study](#)

Abhinav Saxena and Ashutosh Kumar Dubey

Liquid demixing in elastic networks: Cavitation, permeation, or size selection?

PIERRE RONCERAY^{1,2(a)}, SHENG MAO^{3,4}, ANDREJ KOŠMRLJ^{4,5} and MIKKO P. HAATAJA^{4,5(b)}

¹ *Aix Marseille Univ, CNRS, CINAM, Turing Center for Living Systems - Marseille, France*

² *Center for the Physics of Biological Function, Princeton University - Princeton, NJ 08544, USA*

³ *Department of Mechanics and Engineering Science, BIC-ESAT, College of Engineering, Peking University Beijing 100871, PRC*

⁴ *Department of Mechanical and Aerospace Engineering, Princeton University - Princeton, NJ 08544, USA*

⁵ *Princeton Institute of Materials, Princeton University - Princeton, NJ 08544, USA*

received 17 July 2021; accepted in final form 18 February 2022

published online 6 May 2022

Abstract – In cells, phase-separated liquid condensates interact mechanically with surrounding elastic networks such as chromatin and cytoskeleton. By considering the trade-offs between elastic, wetting, and interfacial energies, we theoretically show that three droplet phases can be thermodynamically stable: macroscopic droplets that either cavitate or permeate the network, and mesh-size-limited microdroplets. We show that network strain stiffening further enhances this latter size-limitation effect. Our theory predicts the possibility of yet-unobserved droplet phases in the cytoplasm and nucleoplasm.

editor's choice

Copyright © 2022 EPLA

Demixing of multicomponent biomolecular systems via liquid-liquid phase separation (LLPS) has emerged as a unifying mechanism governing the formation of many membrane-less intracellular bodies (“condensates”) [1–6]. These droplets form in complex environments and often interact with elastic biopolymer networks, both in the cytoplasm (*e.g.*, stress granules and the cytoskeleton) and in the nucleoplasm (*e.g.*, nucleoli and chromatin). While both *in vivo* experiments [7] and studies of synthetic systems [8,9] demonstrate that such macromolecular networks strongly affect LLPS, a fundamental understanding of LLPS in an elastic network is still lacking.

In this letter we show that, upon accounting for capillary forces responsible for network expulsion, small-scale heterogeneity of the network, and its nonlinear mechanical properties, an intriguing picture of the thermodynamics of LLPS in elastic networks emerges. Specifically, we predict that, in addition to the experimentally observed cavitated droplets [7,8] which fully exclude the network, two new stable phases appear: elastically arrested, size-limited droplets at the network pore scale, and network-including macroscopic droplets. We argue that these phases may be relevant for intracellular condensates by rationalizing recent experimental observations of

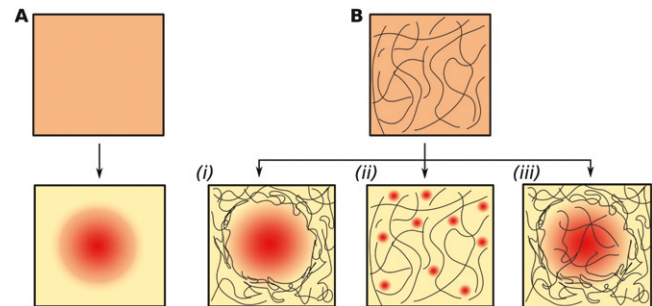


Fig. 1: (A) Classic liquid-liquid phase separation (LLPS) from an initially mixed phase (top) results in a macroscopic droplet of the minority phase (red) immersed in the yellow majority phase (bottom). (B) When LLPS occurs in the presence of an elastic network (top), three possible outcomes are considered (bottom): i) Cavitation. ii) Microdroplets. iii) Permeation of the network into the droplet.

network inclusion [10,11], and predicting the possibility of pore size-limited condensates in chromatin.

When LLPS occurs without mechanical constraints (fig. 1(A)), interfacial energy considerations imply that the thermodynamically stable outcome is a macroscopic spherical droplet of the minority liquid (red) embedded within the majority phase (yellow), with an associated decrease in free energy per unit volume of $\Delta g_0 < 0$. In the presence of an elastic matrix hindering LLPS and

(a) E-mail: pierre.ronceray@univ-amu.fr

(b) E-mail: mhaataja@princeton.edu (corresponding author)

chemically distinct from the two liquids, in contrast, we consider three possible scenarios by which demixing can occur (fig. 1(B)). Each scenario results in a specific free energy cost compared to the reference, unhindered case: i) the minority liquid can create a macroscopic cavity, which incurs an elastic deformation energy penalty E_{el} associated with the network. ii) Alternatively, an extensive number of microdroplets may form within the pores of the network, which avoids elastic deformation but incurs an interfacial energy penalty E_{surf} . iii) Finally, rather than fully excluding the network, the minority droplet can permeate through it, resulting in a wetting energy E_{wet} . Below, we first introduce coarse-grained models that generically capture the physical features of LLPS in an elastic network and employ scaling arguments to evaluate the thermodynamic stability of each phase. To this aim, we assess the free energy penalty per droplet volume $\Delta g_{(i-iii)}$ incurred by the network in each scenario, compared to the reference case of a network-free infinite droplet: assuming that the network does not influence the composition and molar volume of the minority liquid, $\Delta g_{(i-iii)}$ is proportional to the chemical potential of the phase-separated liquid, and thus permits the identification of the most stable scenario. With this approach, we construct a phase diagram for the morphology of phase separation in an elastic network. We then develop a comprehensive theory of such systems based on the continuum mechanical modeling of the network, including finite compressibility and nonlinear strain-stiffening effects. Analytical and numerical approaches are employed to both confirm the salient features of the phase diagram and elucidate the nature of phase transitions between the droplet phases.

We begin by considering scenario i), in which a macroscopic cavity of radius r forms from an initial pore. This scenario has been previously considered for *in vitro* oil-water mixtures in silicone gels [8,9,12] and *in vivo* droplets in the cell nucleus [7]. Within a neo-Hookean (NH) model for network elasticity [7–9], the elastic deformation energy $E_{\text{el}}(r) \sim \frac{4\pi r^3}{3}\alpha G$ scales as the volume of the cavity in the limit $r \rightarrow \infty$. Here, G denotes the shear modulus of the network, while $\alpha \sim \frac{5}{2}$ is a material parameter (see sect. B in the Supplementary Material [Supplementary material.pdf](#) (SM)). This simple behavior describes a broad class of artificial gels [13], while other mechanisms (*e.g.*, detachment of cross-links or fracture at fixed hoop stress [14,15]) can also lead to such a scaling. The free energy per droplet volume penalty is thus

$$\Delta g_{(i)} = \frac{3}{4\pi r^3} E_{\text{el}}(r) \sim \alpha G. \quad (1)$$

We note that $\Delta g_{(i)}$ results in a shift of the demixing phase boundary to lower temperatures [8,16]. Remarkably, this behavior was validated for *in vitro* systems [8], with $\alpha \approx 1.5$. In the presence of macroscopic gradients in the network stiffness, (eq. (1)) also implies that droplet growth is favored in softer regions of the network [7,9,17,18].

While this model captures the macroscopic elastic response of the material, it does not account for small-scale heterogeneities. In both biological and artificial systems considered here, the elastic network is constituted by polymers with a finite pore/mesh size ξ . Consider now scenario ii) in fig. 1(B), in which microdroplets of radius $r \sim \xi$ form within these pores with negligible network deformation. In this case, $E_{\text{el}} \approx 0$, while each microdroplet incurs an interfacial energy penalty $E_{\text{surf}} \sim 4\pi\xi^2\gamma$, where γ denotes the surface tension between the two liquids. This results in a free energy per droplet volume penalty

$$\Delta g_{(ii)} \sim \frac{3\gamma}{\xi}. \quad (2)$$

Comparing eqs. (2) and (1) reveals that in such networks, the trade-off between elastic and interfacial energies is controlled by the *elasto-capillary number* [19]:

$$h \equiv \frac{3\gamma}{\xi G}. \quad (3)$$

When $h < \alpha$, *i.e.*, for large pore sizes and low liquid-liquid surface tensions, the thermodynamically stable phase thus corresponds to the formation of an extensive number of pore-size-limited microdroplets. In contrast, when $h > \alpha$, scenario i) is favored, with macroscopic cavitated droplets whose sizes are not constrained thermodynamically.

Finally, we consider scenario iii) from fig. 1(B): a macroscopic droplet encapsulating a partially excluded network. To assess its thermodynamic stability, we introduce a wetting energy E_{wet} via

$$E_{\text{wet}} = \frac{4\pi r^3}{3}(1 - \varphi)\sigma_p, \quad (4)$$

where φ denotes the fraction of network expelled from the droplet compared to the undeformed state, and σ_p is the *permeation stress*. Microscopically, σ_p arises from differential wetting energy per unit length of the filaments constituting the network in contact with the two fluids [20]. As further discussed in sect. E of the SM, a simple estimate for σ_p can be developed as follows. First, assume that the filaments comprising the network can be approximated as cylinders of radius r_f , corresponding to a liquid-solid interface area per unit length of $\sim 2\pi r_f$. Taking the filaments immersed in the majority liquid (liquid 1) as the reference point, the interfacial energy per unit length of a filament immersed in liquid 2 is thus $\sim 2\pi r_f(\gamma_{2S} - \gamma_{1S})$, where γ_{1S} and γ_{2S} , respectively, denote the interfacial energy between the filament and liquids 1 and 2. Denoting by ρ the volume fraction of the network in its undeformed state, the liquid-network contact area per unit volume is thus $\sim 2\rho/r_f$. Hence, the energy per unit volume difference between the network immersed in liquid 1 and in liquid 2 is $\sigma_p \sim 2\rho(\gamma_{2S} - \gamma_{1S})/r_f$. When $\sigma_p > 0$, the wetting energy of the filaments is lower in the majority liquid phase and filaments are repelled from the minority phase. In contrast, when $\sigma_p < 0$, it is lower in the minority liquid, and phase-separated droplets thus attract the surrounding network. Equation (4) translates this microscopic wetting

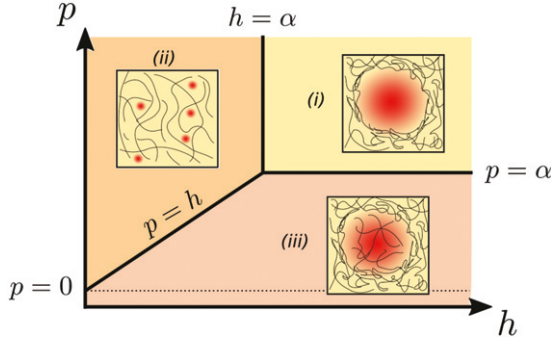


Fig. 2: Droplet phase diagram for LLPS in an elastic network constructed via scaling arguments. The most stable state is indicated in terms of the elasto-capillary h (eq. (3)) and the permeo-elastic p (eq. (6)) numbers. Note that only the dominant contribution to the free energy is retained here, corresponding to eqs. (1), (2) and (5), respectively, for the cavitating i), microdroplet ii), and permeated iii) phases.

phenomenon into a macroscopic effect, which results in a stress discontinuity at the liquid-liquid interface through which the network permeates. Network wetting may also induce an effective change of liquid-liquid surface tension, in particular if the filaments align with the interface; such effects are not considered in the present work.

To proceed with the analysis, we first ignore any σ_p -induced network deformations and set $\varphi = 0$. The free energy cost per volume induced by differential wetting is thus

$$\Delta g_{(iii)} \sim \sigma_p. \quad (5)$$

Comparing eqs. (5) and (1), we find that the thermodynamically stable phase is controlled by a second dimensionless quantity, namely the *permeo-elastic number*

$$p \equiv \frac{\sigma_p}{G}, \quad (6)$$

which is a measure of the degree of network deformation induced by the permeation stress. For $p > \alpha$, scenario i) is the most stable: the repulsion between the network and the minority liquid is sufficiently strong to fully expel the network from the droplet, leading to cavitation. For $p < \alpha$, the droplet permeates through the network rather than excluding it, and scenario iii) is preferred. Finally, when the elasto-capillary number $h < \alpha$, the phase boundary between scenarios ii) and iii) is given by the line $p = h$. The results of the scaling arguments are summarized in a phase diagram in the (p, h) -plane in fig. 2, which identifies the most stable droplet phase. For given material parameters (p, h) , demixing will take place if $\Delta g_{\min} + \Delta g_0 < 0$, where $\Delta g_{\min} = \min[\Delta g_{(i)}, \Delta g_{(ii)}, \Delta g_{(iii)}]$. We note that for scenarios i), ii), the network hinders phase separation and stabilizes the mixed phase; for scenario iii), this depends on the sign of p : for $\sigma_p < 0$, the network prefers the minority phase and favors phase separation.

We have so far considered only the dominant contribution to the free energy for each scenario —either E_{el} ,

E_{surf} or E_{wet} . Network deformation, however, occurs in each of the three scenarios: in ii), microdroplets exert a pressure on the network, while in iii), a permeation stress $\sigma_p > 0$ results in a partial expulsion of the network from the droplet. To quantitatively predict the locations of the phase boundaries and the nature of associated phase transitions, we next discuss the deformation behavior arising from an isolated droplet embedded within a slightly compressible NH network characterized by a stored energy function $W = \frac{G}{2} [I_1 - 2(J-1) + \frac{(J-1)^2}{(1-2\nu)}]$. Here, $I_1 = \lambda_1^2 + \lambda_2^2 + \lambda_3^2$ and $J = \lambda_1 \lambda_2 \lambda_3$ with λ_k denoting the k -th principal stretch, while ν is the Poisson's ratio at small deformation [21].

Examining first scenarios i), ii) for which the network is fully excluded from the droplet, we consider a droplet of radius $r = \lambda_d \xi$ stretching a spherical cavity of initial radius ξ that corresponds to the characteristic pore size of the network (fig. 3(A)). The surface and elastic energy densities are $e_{\text{surf}}(\lambda_d) = \frac{3\gamma}{\lambda_d \xi}$ and $e_{\text{el}}(\lambda_d) = f_{\text{out}}(\lambda_d) \equiv \frac{3}{\lambda_d^3} \min_{t(u)} [\int_1^\infty W(s(u), t(u), t(u)) u^2 du]$, with $s(u)$ and $t(u)$ denoting the radial and hoop stretches at distance $u\xi$ from the origin, subject to the boundary condition $t(1) = \lambda_d$ (see sects. A and B of the SM for derivation details and the perturbative calculation of f_{out}). When the elasto-capillary number h is large (fig. 3(B)), $\Delta g = e_{\text{el}} + e_{\text{surf}}$ decreases monotonically with droplet size r , indicating that cavitation (scenario i) is thermodynamically favored. At small h (fig. 3(C)), in contrast, Δg exhibits a global minimum at $r^* \gtrsim \xi$, corresponding to size-limited microdroplets as per scenario ii). For positive Poisson's ratios ν , r^* increases sharply with the elasto-capillary number h (fig. 3(D)), but remains finite up to the limit of stability of microdroplets, indicating that the cavitation transition i) \rightarrow ii) is weakly first order as surface tension is increased or, equivalently, as the shear modulus of the network is reduced. Interestingly, this transition becomes continuous for auxetic materials with $\nu < 0$ (see sect. C in the SM). We note that when scenario i) is favored, the total free energy of a droplet of size r presents a single maximum at the critical nucleation radius r_c , regardless of the value of Δg_0 . This critical radius may be larger than the mesh size, in which case the nucleation rate is affected by the network. Nucleation and cavitation are thus concomitant in a single “nucleo-cavitation” step in NH materials, and mesh-size-level droplets are fully unstable, rather than being a metastable intermediate (except in a very narrow parameter regime; see SM).

Turning now to the case of a permeated network, we consider a macroscopic droplet (thus neglecting e_{surf}) for which the wetting free energy per volume e_{wet} is a function of fraction $\varphi = 1 - \lambda_i^{-3}$ of the expelled network, where λ_i denotes the homogeneous stretch of the network inside the droplet (fig. 3(E)). In this case, $\Delta g = \min_{\lambda_i} [e_{\text{wet}}(\lambda_i) + e_{\text{el}}(\lambda_i)] = \min_{\lambda_i} [\frac{\sigma_p + W(\lambda_i, \lambda_i, \lambda_i)}{\lambda_i^3} + f_{\text{out}}(\lambda_i)]$ (see sects. A and B in the SM). For large val-

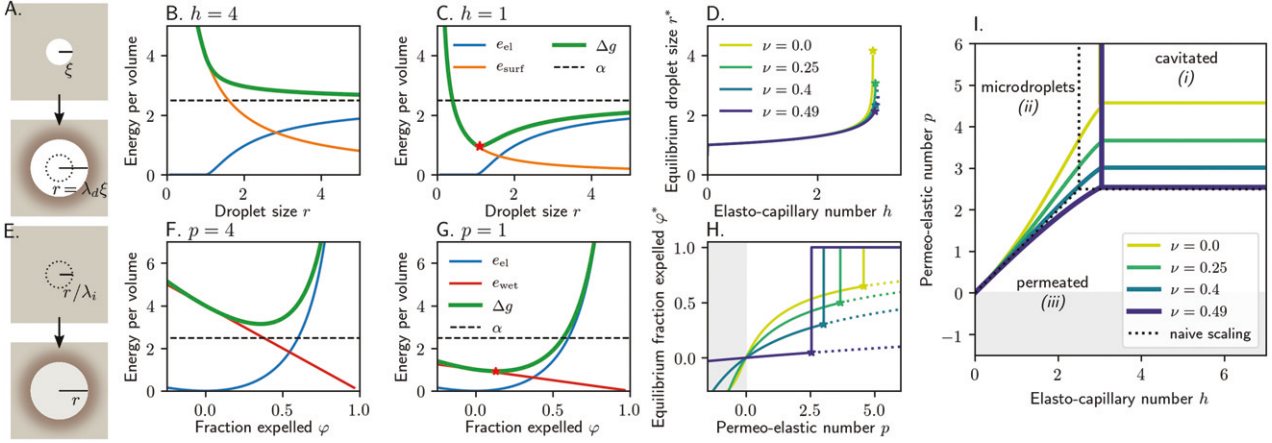


Fig. 3: Analysis of droplet phases within compressible neo-Hookean (NH) networks. (A) Sketch of the geometry of the pore deformation model. (B), (C): elastic energy (blue, e_{el}), surface energy (orange, e_{surf}) and total free energy (green, $\Delta g = e_{\text{el}} + e_{\text{surf}}$) per droplet volume *vs.* droplet size r , respectively for elasto-capillary numbers $h = 4$ (showing monotonic decay of Δg) and $h = 1$ (showing a global minimum of Δg at r^* , red star). Dashed black line indicates the $r \rightarrow \infty$ cavitated limit. (D) Equilibrium droplet size r^* *vs.* h , for different Poisson's ratios ν of the network. Star indicates the limit of stability of phase ii). (E) Sketch of the geometry for the permeation model with inner stretch λ_i . (F), (G): elastic energy, wetting energy (red, e_{wet}) and total free energy (green, $\Delta g = e_{\text{el}} + e_{\text{wet}}$) per volume of a large droplet permeating through the network *vs.* fraction expelled of the network φ , respectively, for permeo-elastic numbers $p = 4$ (where cavitation is favored) and $p = 1$ (with global minimum at φ^* , red star). (H) Equilibrium fraction expelled φ^* *vs.* p . Dashed lines indicate metastable states, with cavitation ($\varphi^* = 1$) energetically favored. (I) Droplet phase diagram in the (p, h) -plane. Dotted lines indicate naive scaling results with $\alpha = 5/2$, as in fig. 2. The shaded area in (F), (G) indicate $p < 0$, *i.e.*, a contractile droplet attracting the network. In (A), (B), (D), (E) we take $\nu = 0.4$. Energy densities and length scales are normalized by the linear shear modulus G and the pore size ξ , respectively.

ues of p , Δg exceeds that of the cavitated case for all φ (fig. 3(F)). In contrast, at low p (fig. 3(G)), the global minimum of Δg occurs at $\varphi^* < 1$, and permeation is favored. When p increases, φ^* increases continuously up to the cavitation point, at which it experiences a compressibility-dependent jump (fig. 3(H)). We summarize these results in a phase diagram for NH materials in fig. 3(I).

While a NH constitutive law describes the deformation behavior of a broad class of materials at finite stretches, many biomolecular networks differ by exhibiting *strain-stiffening* behavior [22–24], whereby the (nominal) tensile stress grows faster than linearly with the stretch. In the permeated case, this nonlinearity limits the exclusion of the network from the droplet, with moderate effects on the phase stability. In contrast, strain stiffening strongly affects phases i) and ii) where the network is fully excluded: the free energy of the cavity grows asymptotically faster than its volume, and the elastic penalty $e_{\text{el}}(r)$ diverges in the limit of large droplets, as illustrated in fig. 4(A) for a minimal model for power-law strain stiffening with an additional nonlinear contribution to stored energy function W given by $\frac{G}{2}[(I_1 - 3)/6\varepsilon_c]^3$. Here, the parameter ε_c controls the strength of the nonlinearity such that NH behavior is recovered in the limit $\varepsilon_c \rightarrow \infty$ (see sect. D in the SM). Thus, effectively $\alpha \rightarrow \infty$, and scenario i) is suppressed: the global energy minimum always occurs at a finite droplet radius r^* , leading to size selection [25]. When the nonlinearity is strong, the equilibrium droplet size $r^* \gtrsim \xi$ even at large capillary forces corresponding to $h \gg 1$ (fig. 4(B), blue), and microdroplets are stable

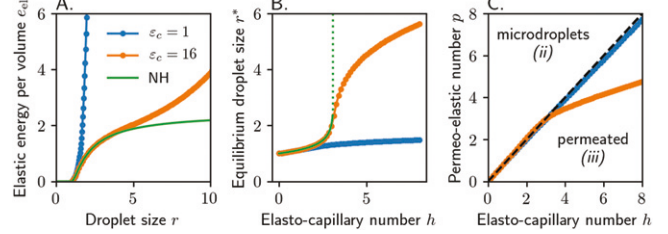


Fig. 4: Numerical analysis of networks with strong (blue) and weak (orange) strain stiffening behavior. The analytical solution for non-stiffening NH materials is also shown (green). (A) Elastic energy per droplet volume as a function of droplet size. (B) Equilibrium droplet size r^* as a function of the elasto-capillary number h . For NH materials, the cavitation transition is indicated by the dotted line. (C) Phase boundary between microdroplets ii) and permeated iii) phases. Cavitation i) is suppressed by the strain stiffening. Dashed line indicates the naive scaling $p = h$.

when $p \gtrsim h$ (fig. 4(C)). When the nonlinearity is weak and emerges only at large stretch, in contrast, microdroplets transition from being linearly arrested with size $r^* \gtrsim \xi$ at $h \lesssim 3$, to being non-linearly arrested at a mesoscopic size $r^* \gg \xi$ at $h \gtrsim 3$ (fig. 4, orange). This transition is a smooth crossover for realistic material parameters, and results in a change of slope of the phase boundary as larger droplets incur a lower surface penalty per unit volume (fig. 4(C)).

In summary, we have demonstrated that liquid-liquid phase separation (LLPS) in an elastic network dis-

Table 1: Order-of-magnitude estimates of the shear modulus G , network mesh size ξ , surface tension γ , and permeation stress σ_p for three classes of experimental systems. The ranges of variation of the elasto-capillary number h and the permeo-elastic number p are shown, and plausible scenarios for LLPS are indicated (most likely ones in bold). Details in sect. F in the SM.

System	G	ξ	γ	σ_p	h	p	Scenarios
I Oil in silicone gel	10^3 – 3.10^5 Pa	2–14 nm	4×10^3 Nm $^{-1}$	10^4 – 3.10^5 Pa	20–700	1.1–6.5	i), iii)
II Cytoplasmic cond.	10–100 Pa	50–150 nm	10^{-6} Nm $^{-1}$	$\pm(0.2$ – $2)$ Pa	0.2–6	$\pm(10^{-3}$ – $0.2)$	ii), iii)
III Nuclear condensates	10 – 10^3 Pa	7–20 nm	10^{-7} – 10^{-6} Nm $^{-1}$	$\pm(10$ – $100)$ Pa	0.01–10	$\pm(0.01$ – $10)$	i), ii), iii)

plays complex morphological diversity at equilibrium. In particular, we have shown that the prevailing picture of cavitated macroscopic droplets is challenged by two alternative scenarios. On the one hand, when the pore-size-level elastic forces dominate the capillary forces, *i.e.*, when the elasto-capillary number h (eq. (3)) is small or when the network displays strong strain-stiffening behavior [25], stable pore-size-limited microdroplets form. We note that this equilibrium size limitation mechanism is distinct from previously considered kinetic limitation effects such as protocol-dependent arrested ripening of cavitated droplets [9,16,18,26] and hindered diffusion of irreversible nanoparticle aggregates in polymer gels [27]. On the other hand, when differential wetting between the network and the two liquids is not strong enough to fully expel the network, *i.e.*, for low permeo-elastic number p (eq. (6)), the network permeates the phase-separated droplets. Employing scaling arguments and continuum mechanics modeling that generically describe LLPS in an elastic network at a coarse-grained level (where the only parameters are the bulk material properties and the pore size), we have constructed a predictive morphological phase diagram that quantifies the equilibrium droplet size and network deformation behavior.

We note that our theoretical predictions rely on several important assumptions. First, we have focused on mechanical and thermodynamic equilibrium states, ignoring kinetic processes such as droplet nucleation [28], ripening [9,18,26] and merging [29], and, in the case of biological systems, their inherently out-of-equilibrium nature. Second, we have ignored all direct interactions between the droplets, which is justifiable when the typical droplet separations are much larger than their size. Third, we have neglected all visco-elastic effects in the network: we thus considered systems over time scales long enough for phase separation to complete, yet short enough for the network to retain its mechanical integrity.

We finally discuss the relevance of the predicted phase diagram for experimental systems by providing estimates for the relevant parameters, presented in table 1. For fluorinated oil demixing in silicone gels (system I with $h \gg \alpha$), consistent with experimental observations [8,9,12], only macroscopic phase separation appears to be relevant: these

networks are too homogeneous, and the surface tension too high, to permit microphase separation. In contrast, for cytoplasmic condensates (system II), low surface tension, large mesh sizes and stiff filaments make permeation the most likely scenario, while cavitation appears to be ruled out by our theory: if droplets exclude the cytoskeleton, they are likely to be size selected at the network mesh size. In the context of intracellular phase separation in the nucleoplasm (III), all three scenarios are possible. In particular, DNA is only partially expelled from nucleoli [10], suggesting that these organelles may operate in the permeated regime with $p > 0$. Intriguingly, recent studies show that phase separation of HP1a leads to the formation of DNA-rich heterochromatin domains [11], suggesting a network-attracting permeated phase with $p < 0$. Finally, we predict that mesh-size-selected microdroplets are also possible in chromatin. Interestingly, the chromatin mesh size is well below the optical resolution limit: if such a phase exists, it may not have been fully characterized yet. For instance, it was recently proposed that phase-separated condensates are involved in the activation and repression of gene transcription [30–32]. Our work suggests that such condensates might be elastically limited by the mechanisms presented herein.

These order-of-magnitude estimates suggest that further super-resolution microscopy studies are needed to fully characterize intracellular LLPS, focusing both on the presence of network inclusion within membraneless condensates, and on the possible existence of elastically limited nanodroplets. We have also shown that existing synthetic systems for LLPS in elastic networks [8,9,12] operate in a parameter regime that is vastly different from intracellular LLPS (table 1). Our work provides design principles for new biomimetic systems which capture properties of *in vivo* systems more faithfully.

These engineered systems could be also useful for nanofabrication, as well as to serve as crucibles for chemical reactions favored by phase exchange: the very high surface-to-volume ratio would permit fast exchange between the two phases. The multi-stage chemical reactions can be guided in structured multi-phase droplets, such as is the case with the ribosome biogenesis in nucleoli [6], where the internal organization of phases is dictated by

their surface tensions [33]. Finally, our study underscores the importance of a novel quantity, the permeation stress σ_p , on LLPS. While we have focused on the case of droplets that (partially) expel the network, our theory predicts that capillary forces are reversed when $\sigma_p < 0$: in this case, the network facilitates phase separation and condenses around the droplets. Such network-droplet attraction could, *e.g.*, couple to the nonlinear mechanics of fiber networks to result in large-scale stresses [34,35], as well as yield new physical insights into the structure and function of biomolecular condensates.

SM is supported by Beijing Innovation Center for Engineering Science and Advanced Technology (BIC-ESAT) at Peking University. SM, AK and MPH are supported by NSF through the Princeton University Materials Research Science and Engineering Center DMR-2011750. MPH also acknowledges support from a Princeton University Focused Research Team award on Engineering Living Organelles. PR is supported by the NSF through the Center for the Physics of Biological Function (PHY-1734030), by the “Investissements d’Avenir” French Government program managed by the French National Research Agency (ANR-16-CONV-0001) and by the Excellence Initiative of Aix-Marseille University - A*MIDEX.

Data availability statement: All data that support the findings of this study are included within the article (and any supplementary files).

REFERENCES

- [1] BRANGWYNNE C. P., ECKMANN C. R., COURSON D. S., RYBARSKA A., HOEGE C., GHARAKHANI J., JÜLICHER F. and HYMAN A. A., *Science*, **324** (2009) 1729.
- [2] ALBERTI S., GLADFELTER A. and MITTAG T., *Cell*, **176** (2019) 419.
- [3] HYMAN A. A., WEBER C. A. and JÜLICHER F., *Annu. Rev. Cell Develop. Biol.*, **30** (2014) 39.
- [4] BERRY J., BRANGWYNNE C. P. and HAATAJA M., *Rep. Prog. Phys.*, **81** (2018) 046601.
- [5] CHOI J.-M., HOLEHOUSE A. S. and PAPPU R. V., *Annu. Rev. Biophys.*, **49** (2020) 107.
- [6] FERIC M., VAIDYA N., HARMON T. S., MITREA D. M., ZHU L., RICHARDSON T. M., KRIWACKI R. W., PAPPU R. V. and BRANGWYNNE C. P., *Cell*, **165** (2016) 1686.
- [7] SHIN Y., CHANG Y.-C., LEE D. S. W., BERRY J., SANDERS D. W., RONCERAY P., WINGREEN N. S., HAATAJA M. and BRANGWYNNE C. P., *Cell*, **175** (2018) 1481.
- [8] STYLE R. W., SAI T., FANELLI N., IJAVI M., SMITH-MANNSCHOTT K., XU Q., WILEN L. A. and DUFRESNE E. R., *Phys. Rev. X*, **8** (2018) 011028.
- [9] ROSOWSKI K. A., SAI T., VIDAL-HENRIQUEZ E., ZWICKER D., STYLE R. W. and DUFRESNE E. R., *Nat. Phys.*, **16** (2020) 422.
- [10] SLUIS M. v., VUUREN C. v., MANGAN H. and MCSTAY B., *Proc. Natl. Acad. Sci. U.S.A.*, **117** (2020) 10368.
- [11] STROM A. R., EMELYANOV A. V., MIR M., FYODOROV D. V., DARZACQ X. and KARPEN G. H., *Nature*, **547** (2017) 241.
- [12] KIM J. Y., LIU Z., WEON B. M., COHEN T., HUI C.-Y., DUFRESNE E. R. and STYLE R. W., *Sci. Adv.*, **6** (2020) eaaz0418.
- [13] TRELOAR L. R. G., *The Physics of Rubber Elasticity*, third edition, *Edition Oxford Classic Texts in the Physical Sciences* (Oxford University Press, Oxford, NY) 2005.
- [14] RAAYAI-ARDAKANI S., EARL D. R. and COHEN T., *Soft Matter*, **15** (2019) 4999.
- [15] VIDAL-HENRIQUEZ E. and ZWICKER D., *Proc. Natl. Acad. Sci. U.S.A.*, **118** (2021) e2102014118.
- [16] KOTHARI M. and COHEN T., *J. Mech. Phys. Solids*, **145** (2020) 104153.
- [17] VIDAL-HENRIQUEZ E. and ZWICKER D., *Soft Matter*, **16** (2020) 5898.
- [18] ROSOWSKI K., VIDAL-HENRIQUEZ E., ZWICKER D., STYLE R. W. and DUFRESNE E. R., *Soft Matter*, **16** (2020) 5892.
- [19] SHAO X., FREDERICKS S. A., SAYLOR J. R. and BOSTWICK J. B., *Phys. Rev. Lett.*, **123** (2019) 188002.
- [20] DE GENNES P. G., *J. Phys. Chem.*, **88** (1984) 6469.
- [21] BIWA S., *Int. J. Non-Linear Mech.*, **41** (2006) 1084.
- [22] OGDEN R. W., *Non-linear Elastic Deformations* (Courier Corporation) 1997.
- [23] STORM C., PASTORE J. J., MACKINTOSH F. C., LUBENSKY T. C. and JANMEY P. A., *Nature*, **435** (2005) 191.
- [24] ERK K. A., HENDERSON K. J. and SHULL K. R., *Biomacromolecules*, **11** (2010) 1358.
- [25] WEI X., ZHOU J., WANG Y. and MENG F., *Phys. Rev. Lett.*, **125** (2020) 268001.
- [26] ZHANG Y., LEE D. S. W., MEIR Y., BRANGWYNNE C. P. and WINGREEN N. S., *Phys. Rev. Lett.*, **126** (2021) 258102.
- [27] LAXTON P. B. and BERG J. C., *Langmuir*, **24** (2008) 9268.
- [28] SHIMOBAYASHI S. F., RONCERAY P., SANDERS D. W., HAATAJA M. P. and BRANGWYNNE C. P., *Nature*, **599** (2021) 503.
- [29] LEE D. S. W., WINGREEN N. S. and BRANGWYNNE C. P., *Nat. Phys.*, **17** (2021) 531.
- [30] CHO W.-K., SPILLE J.-H., HECHT M., LEE C., LI C., GRUBE V. and CISSE I. I., *Science*, **361** (2018) 412.
- [31] SABARI B. R., DALL’AGNESE A., BOIJA A., KLEIN I. A., COFFEY E. L., SHRINIVAS K., ABRAHAM B. J., HANNETT N. M., ZAMUDIO A. V., MANTEIGA J. C., LI C. H., GUO Y. E., DAY D. S., SCHUIJERS J., VASILE E., MALIK S., HNISZ D., LEE T. I., CISSE I. I., ROEDER R. G., SHARP P. A., CHAKRABORTY A. K. and YOUNG R. A., *Science*, **361** (2018) eaar3958.
- [32] TREEN N., SHIMOBAYASHI S. F., Eeftens J. *et al.*, *Nat. Commun.*, **12** (2021) 1561.
- [33] MAO S., CHAKRAVERTI-WUERTHWEIN M. S., GAUDIO H. and KOŠMRLJ A., *Phys. Rev. Lett.*, **125** (2020) 218003.
- [34] RONCERAY P., BROEDERSZ C. P. and LENZ M., *Proc. Natl. Acad. Sci. U.S.A.*, **113** (2016) 2827.
- [35] RONCERAY P., P. BROEDERSZ C. and LENZ M., *Soft Matter*, **15** (2019) 331.